Topo-bathymetric airborne LiDAR for fluvial-geomorphology analysis

Dimitri Lague, Baptiste Feldmann

Final submitted version of :

Topo-bathymetric airborne lidar for fluvial-geomorphology analysis

Dimitri Lague[a], **Baptiste Feldmann**[b]

a: Univ Rennes, CNRS, Géosciences Rennes, UMR 6118, Rennes, France

b: Univ Rennes, CNRS, Nantes-Rennes Topo-Bathymetric Lidar platform, OSUR, UMS 3343, Rennes, France

Chapter 2 of Developments in Earth Surface Processes, Volume 23, 2020, pp. xi-xii

Final published version available here: https://doi.org/10.1016/B978-0-444-64177-9.00002-3

Abstract

Topographic airborne lidar using a near-infrared laser cannot penetrate water. A new generation of topo-bathymetric sensors adds a green laser to measure shallow bathymetry. We synthesize previous work and present new results using these sensors in the context of fluvial geomorphology. These sensors allow synoptic continuous topography and bathymetry with a vertical accuracy better than 10 cm and a capacity to resolve details of 20-30 cm. The maximum measurable depth can vary from one to six meters depending on water turbidity, bottom reflectance, and the sensor used. Based on a 55 km survey of the Ain river (France), we illustrate the level of detail recorded in raw data, the full waveform record, and the challenges in detecting individual bathymetric points that require a refraction correction amongst billions of points. We show various applications, including synoptic measurement of erosion/sedimentation, back calculation of water optical properties, and large-scale, high-resolution mapping of inundation patterns.

Keywords : lidar, river, green laser, bathymetry, erosion

1. High Resolution Topography: where is the bathymetry?

Geomorphology has been profoundly transformed by the advent of high-resolution topography (HRT) obtained from methods such as topographic airborne lidar (ALS), terrestrial lidar, and structure From motion (SFM) (e.g., Glennie et al., 2013; Passalacqua et al., 2015; Tarolli, 2014). This transformation stems from the unique combination of four characteristics typical of HRT data: they are 3-dimensional, high resolution, high precision and synoptic. For all the information they contain on landscape and vegetation geometry across a large range of scales, they lack a key characteristic when it comes to fluvial environments: the ability to measure river bathymetry and other water bodies with the same four key characteristics.

In particular, topographic airborne lidar typically uses an infrared wavelength laser (λ = 1064 nm or 1550 nm). This wavelength cannot penetrate water and returns of the water-surface position are very weak, if there are returns at all, when operated at elevations (>1000 m) typical of topographic lidar survey. Interpolated DEMs give the false impression that “something” exists where water bodies are, but raw topographic lidar generally contains no signal on water bodies. The geomorphological analysis can thus only be done on the dry part of the topography, which might be acceptable in the case of very shallow rivers, but rapidly degrades with river depth, or when the extent of shallow water is very large, such as in a braided river. The fluvial geomorphologist is generally left with no, or sparse data corresponding to traditional cross-sections (sonar or GPS) and 2D imagery. This is a severe limitation given that most of the geomorphic activity of rivers is embodied in bedload sediment transport, bedform mobility, and erosion of the bank toe, all of which are features of, or occur in the deepest, permanently wet, part of the channel. This limitation at the reach scale propagates over the entire drainage network when it comes to evaluate sediment and nutrient transfers, flood propagation, fish habitats, or to predict the impacts of dam removal/creation. For these key questions, large-scale, high-resolution, 2D hydro-

sedimentary modelling becomes feasible (Davy et al., 2017), but it cannot proceed if the bathymetric information needed to feed the models is missing.

Poised by the lack of 3D seamless, high-resolution, land-water data in fluvial environments, various techniques have been tested and developed in the last two decades. One of the most promising is airborne, lidar topo-bathymetry (ALTB) dedicated to shallow water environments. Here, we synthesize recent work, and report on 3 years of deployment of such a sensor on various rivers and water bodies, highlighting limitations, challenges in data processing and opportunities offered by this new type of data.

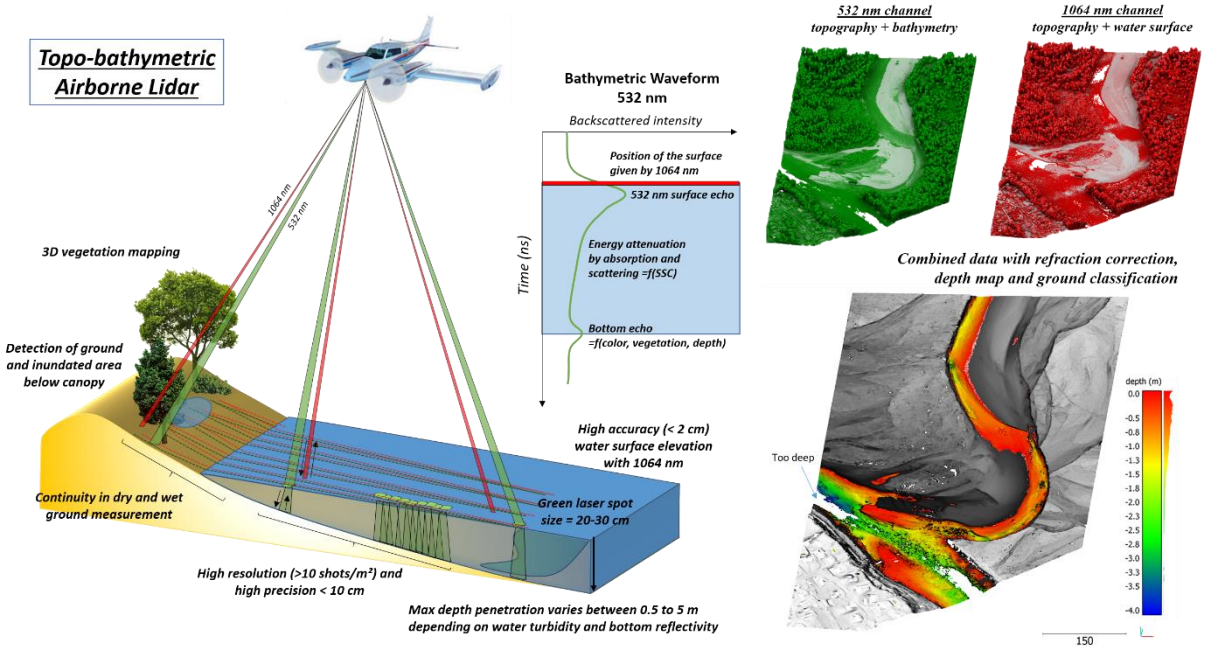

Figure 1: Principle of topo-bathymetric airborne lidar with the scanning geometry of the Teledyne Optech Titan DW and main capabilities. An ideal bathymetric waveform is shown on the right. Discrete echoes would correspond to the two peaks appearing in the signal corresponding to a surface echo and the bottom echo. Right: illustration of the two point clouds (532 nm and 1064 nm) produced by the instrument at the confluence between the Ain and the Rhône (France), and the continuous topo-bathymetric, point-cloud data after automatic land-water classification, refraction correction for bathymetric points, and ground detection for the topography. The Ain bathymetry is fully covered, but the Rhône is only measured down to 4 m depth resulting in partial bathymetric cover (see also Fig. 5)

2. Synoptic fluvial bathymetry survey techniques

2.1 Topo-bathymetric lidar vs existing approaches

Apart from ALTB, four main techniques have been tested or developed to measure fluvial bathymetry at high resolution (i.e., at least 1 pt/m²) and synoptically. They differ in their depth capability and the simultaneous measurement of emerged topography and vegetation (Table 1):

1**. Spectral methods** use the difference in absorption of the different wavelengths of visible light to estimate water depth. They use either high-resolution, multispectral or hyperspectral, aerial or satellite images (e.g., Legleiter, Roberts, & Lawrence, 2009; Lejot et al., 2007). Being a passive optical measurement, this approach is restricted to shallow, clear-flowing streams with a perfectly visible bottom. Depths up to 2-2.5 m have been measured in rivers with a mean error of the order of 15-20 cm (e.g., Legleiter et al., 2016). The approach generally requires independent depth measurements for calibration. Spectral methods now benefit from low cost deployment from small unmanned aerial systems (UAS) and the development of compact, multispectral and hyperspectral cameras. It is, however, sensitive to direct (i.e., screening), or indirect (i.e., light intensity variations), shading effects

due to vegetation, as well as surface waves. The method, based on 2D imagery does not natively capture the 3D geometry of ground and vegetation, although it can now be combined with SFM UAS surveys to get high resolution 3D topography if vegetation cover is not too dense, or with existing airborne lidar or mobile lidar surveys (e.g., Williams et al., 2014).

2. **Multi-beam sonar** (MBS) can only be used for navigable and deep watercourses (> 3 m) and remains the only solution for synoptic bathymetric surveys of deep, wide rivers with very low water clarity (Leyland et al., 2017; Nittrouer et al., 2008; Parsons et al., 2005). Mobilization costs are high, even though decreasing sensor size, and the availability of unmanned surface vehicles may significantly reduce costs in the near future. Although precision and spatial resolution are of centimetric range on the channel bed, MBS cannot generally measure submerged river banks unless coupled with a side-mounted, multibeam sounder. Surrounding topography and vegetation cannot be measured unless coupled with a mobile terrestrial lidar (e.g., Leyland et al., 2017).

3. **Bathymetric Structure From Motion:** following early attempts at stereo photogrammetry conducted through water (Westaway et al., 2000), this recent technique exploits the capacity of SFM algorithms dedicated to 3D topographic reconstruction using UAS imagery to also reconstruct the underwater 3D geometry of shallow, clear-water rivers (Woodget et al., 2015). Because SFM algorithms do not factor in the light refraction at the air/water interface, the apparent depth is shallower than the true depth. Correction methods have begun to be developed (Dietrich, 2017; Woodget et al., 2015). They show promising results with precision and accuracy on par with SFM data on dry land (0.01-0.02 % of the flying height) and maximum depth of 1 to 2 m. Although this new method potentially suffers from the same limitations that spectral methods do when it comes to water clarity, surface waves, and depth limitation, it has the advantage of directly generating a continuous topo-bathymetric survey. As with UAS-SFM surveys, dense riparian vegetation presents a challenge to accurately measure ground and bathymetry (Table 1).

Table 1: Methods used for acquisition of synoptic, high-resolution topography in fluvial environments over reaches longer than 1 km. Measure type: -: impossible, + : possible , ++ : suitable

	Topo	**Vegetation**	**Shallow rivers (< 3 m)**	**Deep rivers (> 3 m)**	**Survey extent**	**Survey Cost[1]**
Topographic airborne Lidar	++	++	-	-	> 10 km	€€
Bathymetric SFM	++	+	+[2,3]	-	< 10 km	€
Spectral methods	-	-	+[3]	-	1 – 100 km	€-€€[4]
Multibeam sonar + mobile lidar	+	+	-	++	1-10 km	€€-€€€
Topo-bathy airborne Lidar	++	++	++	+[5]	> 10 km	€€€

1: total survey cost, meaning that the ranking of cost per km can be different depending on the total survey extent. 2: currently being developed (Dietrich, 2017; Woodget et al., 2015). 3: limited by bottom visibility, vegetation shadow and surface waves; 4: cost depends on imagery type (multispectral, hyperspectral) and deployment platform (drone, airplane, satellite) and includes ground calibration. 5: only in clear water with clear river bed

4**. Coastal bathymetric airborne lidar** has been employed by researchers for decades (e.g., Guenther, 1985; Guenther et al., 2000). These sensors use a powerful green laser ($\lambda = 532$ nm) that is amongst the least absorbed wavelength in water and can measure depths up to 40-50 m in very clear waters and clear bottoms. Their use in the context of river surveying remains, however, limited (Bailly et al., 2010;

Hilldale et al., 2007) for three reasons: (i) the mobilization cost is very high; it is greater than 1000 - 2000 € / km²; (ii) the laser footprint is 1 to 2 m in diameter, which coupled with a low point density (e.g., 0.1-1 pts / m²), results in a measurement resolution that is too coarse for small to medium-sized streams. Similarly the topographic and vegetation records are too coarse compared to the requirement of modern topographic airborne lidar data; (iii) owing to a high power pulse of longer duration, the detection of shallow depths (<0.5 m) is difficult (Allouis et al., 2010) which is a strong limitation for shallow rivers surveys.

2.2 Topo-bathymetric airborne lidar sensors

To overcome the limitations of deep bathymetric sensors in terms of resolution, shallow-depth measurement, and deployment cost, a new generation of green lidar sensors has been developed over the last decade. These new sensors are characterized by a narrow laser beam of lower power that allows a higher shot frequency and a shorter pulse duration. After a first prototype by NASA (EEARL-A followed by EEARL-B) which demonstrated the interest of this approach for fluvial bathymetric mapping (e.g., Daniele et al., 2018; McKean et al., 2009), the principal manufacturers of airborne lidar equipment (Teledyne Optech, Leica, Riegl) have produced sensors that are now at their second generation. They all share similar characteristics (Figure 1): a narrow green laser beam (λ = 532 nm) resulting in laser spot size of ~ 20-30 cm on the water surface, and low power allowing high shot frequency (> 100 khz), resulting in point density greater than 5 pts/m². All tpo-bathymetric sensors need to be deployed at survey elevations above ground level (AGL) lower than 600 m for the backscattered laser beam to be focused enough, with typical AGL of 300-400 m to maximize depth penetration. At this AGL the swath is 180 to 250 m wide depending on the sensor. The low AGL is the main difference with topographic lidar, which can be deployed at much higher elevation. Combined with a more complex post-processing of the data (see section 4), this results in ALTB surveys having higher costs/km² than topographic lidar, but are considerably cheaper than ALB. Sensors will differ by their scanning patterns, emitted pulse energy, and backscattered signal processing, which will impact the maximum detectable depth (see section 3.2). They will all offer the possibility of recording the entire backscattered signal for each shot, called full waveform (FWF), for reanalysis after the flight, on top of discrete echoes that are detected onboard (figure 1 and 2).

First generation sensors only used a green laser (Fernandez-Diaz et al., 2014; Mandlburger et al., 2015; McKean et al., 2009; Pan et al., 2015), combined occasionally with a second survey using a topographic lidar (e.g., Pan et al., 2015). A new generation sensor now uses an additional laser beam at λ = 1064 nm within the same sensor, which is essential to accurately measure water surface elevation, automatically classify wetted areas, and to increase point-density on dry surfaces as the green laser operates as a normal topographic lidar as well (figure 1). These new sensors will also integrate an aerial camera to generate high resolution orthophotos.

2.3 Survey examples and typical data characteristics

This work presents new data acquired with a Titan DW instrument (Dual Wavelength λ = 1064 nm and λ = 532 nm) developed by Teledyne-Optech in 2014 (Figure 1). It is operated since 2015 by the University of Nantes and Rennes in France with a focus on river topo-bathymetry and monitoring of coastal environments. It also exists in a version with a third wavelength (λ = 1550 nm) operated by the National Center for Airborne Laser Mapping in the US since 2014 (Fernandez-Diaz et al., 2016), with several datasets available for download on OpenTopography. Except for the specific green wavelength, classification of wet areas, and the correction of refraction of bathymetric echoes (see section 4), the sensor operation and data processing are similar to traditional topographic airborne lidar. The reader interested in better understanding airborne lidar operation, data processing, and error budget is referred to dedicated books (e.g., Vosselman & Maas, 2010).

We present results from 2 surveys of the Ain river (e.g., Lassettre et al., 2008) located in the eastern part of France (figures 1, 2) that were flown for Electricité de France. The first survey in July 2015 consisted of 42 km of river length between the Poncin dam and the confluence with the Rhone. This survey required 7 hours of acquisition (1.5 days of operations), resulting in 12 billion points (532 nm + 1064 nm) to process. The second survey in September 2016 added 18 km of river length survey, including 6 km that were already surveyed near the confluence with the Rhône. Our results and recommendations also include expertise gathered from surveying other rivers in France with various characteristics: low energy streams with dense riparian and aquatic vegetation (Connie, Sélune), intermediate-size, gravel-bed rivers with mobile bed (Vieux Rhin, Moselle), and a large sand-bedded braided section of the Loire river.

When operated for topo-bathymetric surveys, the Titan DW is flown at an AGL ranging from 330 to 400 m, at a flight speed of 200 km/h, and a shot frequency of 200 khz on each channel. This results in typical point densities of 36 pts/m² on land (532 nm + 1064 nm), and 18 pts/m² for the bathymey (532 nm) on a single pass. Depending on the project specifications, an overlap of 20 to 50 % is imposed between flight lines, which can result in up to twice the point density. A digitizer is associated to the Titan DW to record the full waveform (FWF) data of the 532 nm channel at shot frequencies ranging from 100 khz to 200 khz depending on the mission requirements. As fluvial corridors are generally winding and the flight line swath is of the order of 150-200 m, complex flight plans are required to minimize acquisition time and total cost. The green laser is pitched by 7° forward to avoid strong surface reflection on water that would blind the sensor if the incidence angle is too small. The 1064 nm laser has no forward pitch to better detect the water surface. Accurate calibration of the two laser-beam geometries is essential to get geometrically consistent 532 nm and 1064 nm point clouds (Figure 1). For the Titan, it proved to be stable over the 3 years of operation, with less than 1 cm mean difference of vertical and horizontal positioning measured on hard horizontal and vertical surfaces.

Trajectory and attitude of the instrument are computed using a high quality integrated inertial measurement unit and GNSS system. The trajectory is post-processed using a combination of the permanent French GNSS network (IGN RGP) and precise point positioning resulting in typical uncertainty on trajectory position ranging from 2 cm to 5 cm in (X,Y,Z) without any temporary GNSS base station on the ground. Given the low flight elevation in topo-bathymery, the vertical accuracy before any ground control adjustment is better than 20 cm and is generally better than 5 cm when adjusted with ground control. The precision on flat hard surfaces, measured over a 0.5 m radius disk as the standard deviation of point distance to a mean plane, is less than 3 cm for both channels. The accuracy and precision of the bathymetric point is presented in the next section.

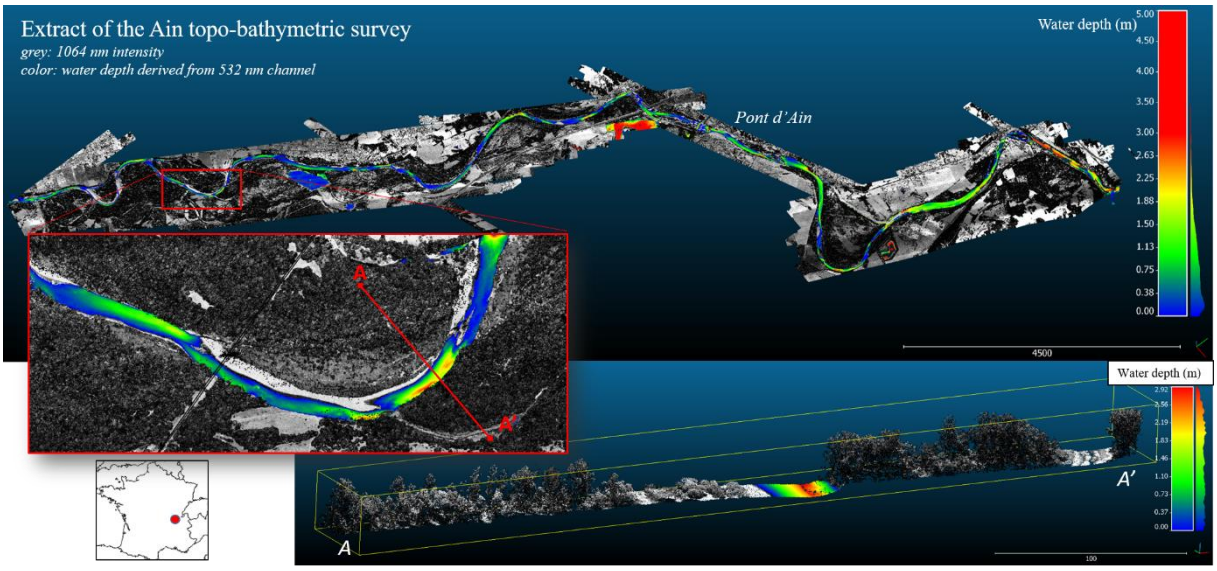

Figure 2: A 13 km extract of the 53 km long Ain topo-bathymetric survey. Data courtesy of Electricité de France. The mean point density, including line overlap, is 29 pts/m² below water and 59 pts/m² above.

3. Controls on depth penetration and surveyable rivers

A critical aspect of topo-bathymetric lidar is the maximum measurable depth $D_{max,}$ which remains, to date, difficult to predict *a priori* for a given river and sensor. In the following, we discuss the parameters controlling D_{max}, we introduce a new way to evaluate some of the parameters controlling D_{max}, and we synthesize previous results and our own experience to evaluate the suitability of ALTB for various type of rivers, including recommendation on the best survey season.

3.1 Theoretical controls on bathymetric waveform and bottom echo intensity

Several factors will control the amount of light energy reflected from the bottom of a river, which ultimately controls the maximum measurable depth (e.g., Abdallah et al., 2012; Guenther, 1985). These factors can be understood by studying a bathymetric waveform (Figure 4.1) that corresponds to the backscattered signal received by the instrument from which it will detect the main discrete echoes, and which can also be independently recorded, typically at a frequency of 1 Mhz for further reanalysis. The actual waveform will vary with the instrument due to different impulse duration and shape, but the overall geometry will be similar. In deep water (> 2 m), a bathymetric waveform has 3 components (Figure 3):

1. **A surface echo** whose peak can be shifted in depth by several tens of centimeters from the true surface of the water and whose intensity varies due to complex optical interactions with the roughness of the water surface (e.g., waves, turbulence) and water clarity (Guenther, 1985; Mandlburger et al., 2013; Pan et al., 2015; Zhao et al., 2018). Water-surface roughness will tend to increase the reflection component of the incident laser, with a directionality dependent on roughness anisotropy (Legleiter & Fonstad, 2012). Although theoretical models exists for oceanic environments to account for the role of waves (e.g., Abdallah et al., 2012), the prediction of transmission loss and of the vertical shift of peak energy for the specific conditions of rivers remains largely unknown. Quite importantly, any vegetation cover on the surface of the water (e.g., duckweeds) or above the water (riparian vegetation) will limit the energy transmitted in the water column and the bathymetric capacities. Similarly, areas of white water will backscatter most of the emitted energy due to air bubbles, with no energy left to measure the bathymetry.
2. **An exponential attenuation of the signal** in the water column due to a combination of absorption by water and dissolved substance, and scattering by suspended organo-detritic particles and air bubbles, including backscattering towards the sensor (Abdallah et al., 2012; Cossio et al., 2009; Legleiter & Fonstad, 2012). The scattering component is expected to be dominant in rivers for two reasons. First, at the considered wavelength, the scattering coefficient of suspended particle should be several times larger than the absorption coefficient (Legleiter et al., 2016; Legleiter & Fonstad, 2012). Second, the narrow beam and small receiver-area configuration of topo-bathymetric sensors

is very sensitive to scattering that spreads out the laser spot in the water column, thus reducing the energy received by the narrow field of view of the sensor. This is a major difference with coastal bathymetric sensors that are more sensitive to absorption (Guenther et al., 2000). The exponential decay of the energy can be characterized by the light attenuation coefficient $K_{d,532\ nm}$ (m^{-1}) specific to the wavelength 532 nm. For narrow aperture sensors, $K_{d,532\ nm}$ should be equal to the beam attenuation coefficient *c(532)* which is the sum of the absorption and scattering coefficients (Cossio et al., 2009). This, however, has not yet been formally demonstrated with field data. Quantitative relationships between $K_{d,532\ nm}$ and turbidity are not known in rivers, but K_d will increase with the concentration in suspended inorganic and organic particles. An empirical proxy for water clarity can be obtained from Secchi disk depth (SDD) measurements, in which a 30 cm black and white disk is lowered down in water. The depth at which the disk is no longer visible is the SDD. SDD is generally used by manufacturers to specify the depth penetration of bathymetric sensors for a given bottom reflectivity. SDD measurements have been calibrated to the sunlight attenuation (i.e., downwelling irradiance) K_d in coastal environments (e.g., Devlin et al., 2008; Ee et al., 2017; Lee, 2018) and to suspended sediment concentration, however only very limited work has been done to evaluate these relationships in rivers (Davies-Colley & Nagels, 2008), and how $K_{d,\ 532\ nm}$ varies with K_d or SDD.

3. **A bottom echo** whose backscattered energy will be proportional to the bed reflectivity at a 532 nm wavelength. Legleiter and co-authors (2009) have measured reflectivity as low as 0.05 for wet gravel and periphyton, defined as the complex mixture of algae, biofilms and detritus attached to the river bed. Beyond this work, the wetted bed reflectivity remains largely underconstrained in rivers. The geometry of the illuminated target is also important: a flat sandy surface behaving as a diffuse reflector is optimum, whereas aquatic vegetation acts as a complex porous reflector that may stretch the laser pulse over the aquatic canopy height and reduce the likelihood of detecting a peak. Hence, aquatic vegetation is in general very detrimental to river bathymetric survey. If too much energy has been lost travelling in water due to turbidity or depth, the bottom echo can be smaller than the noise level of the instrument, and the bed cannot be detected.

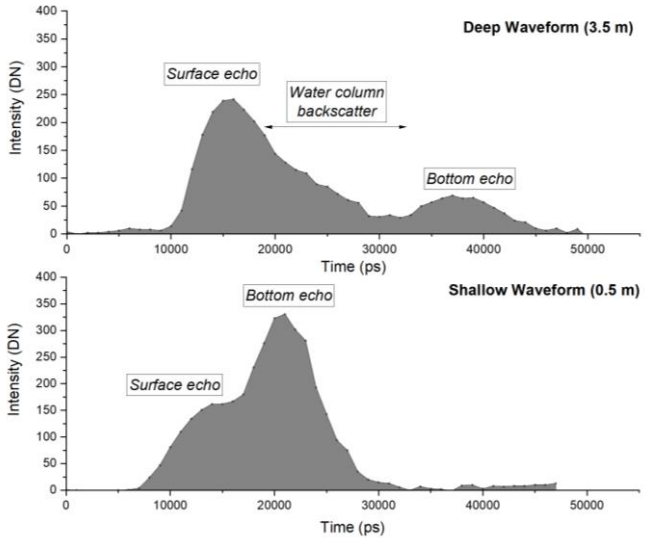

Figure 4: Raw waveform records from the Titan DW 532 nm channel corresponding to the cross-section shown in Figure 4 (uncorrected from light celerity difference in water (see section 4)). The intensity is given in digital number (an electronic measure without unit). **a**: deep water part in the center of the channel. **b**: shallow area near the channel banks.

Figure 4 shows the 3D waveform intensity field corresponding to each sample of the full waveform record of the 532 nm laser (effectively an x,y,z point with an intensity), and computed with a new plugin we have developed in CloudCompare (EDF R&D, 2011). This represents the raw backscattered signal on which the sensor detects maxima in real time to produce the so-called discrete echoes (Figure 1b), or after which a reanalysis of the FWF can be performed to detect weak echoes corresponding to deeper points. Figure 4 shows several key characteristics of topo-bathymetric lidar:

- Bathymetric echoes have very little backscattered energy compared to dry surfaces. Figure 4a shows strong dissipation of energy in the water column in the middle of the river such that the deepest points have a backscattered energy more than 10 to 20 times smaller than a dry ground echo. This makes the detection of these echoes challenging. Figure 4b shows that discrete bathymetric echoes are detected down to 2.05 m depth in this part of the River Ain, but a very simple reanalysis of the FWF data detect weak echoes down to 3 m, albeit with additional noise and false detection within the water column (figure 4d).
- Topo-bathymetric point clouds are perfectly continuous between the dry and wetted area (Figures 1, 4c), an essential characteristic related to their short pulse duration. Coastal bathymetric sensors are not able to achieve this key feature of topo-bathymetric sensors (Allouis et al., 2010). This originates from the bottom echo intensity being always larger than the surface echo at very shallow depth in clear rivers (< 50 cm, Figure 3b), and will be the one detected when echoes overlap. On the contrary, on turbid environments, or in near-shore, coastal environments, the surface echo might be significantly larger than the bottom echo, making the detection of shallow areas (< 50 cm) very difficult. In this example, flown in summer, screening by riparian vegetation reduces the amount of energy reaching the water surface resulting in smaller point density near the banks.
- The peak of surface energy in Figure 4a is on average between 0 and 40 cm below the water surface which is itself precisely captured by the 1064 nm channel. As a consequence, discrete echoes and FWF echoes in the 532 nm do not give an accurate position of the water surface (Mandlburger et al., 2015; Pan et al., 2015). In this example they are spread between 0 and 38 cm. The use of an additional 1064 nm channel precisely measuring the water surface elevation is thus essential for accurate refraction correction (Guenther et al., 2000). As shown in Figure 4b, the 1064 nm and 532 nm are perfectly co-registered on dry flat surfaces. Given that the 1064 nm laser does not penetrate water, it provides a very accurate measure of the water elevation that we estimate at +-2 cm, the measured precision of the data on lake surfaces. However, the 1064 nm surface echoes are not as continuous as the 532 nm echoes due to specular reflection at high incidence angles and subtle variations in the characteristics of the water surface roughness.

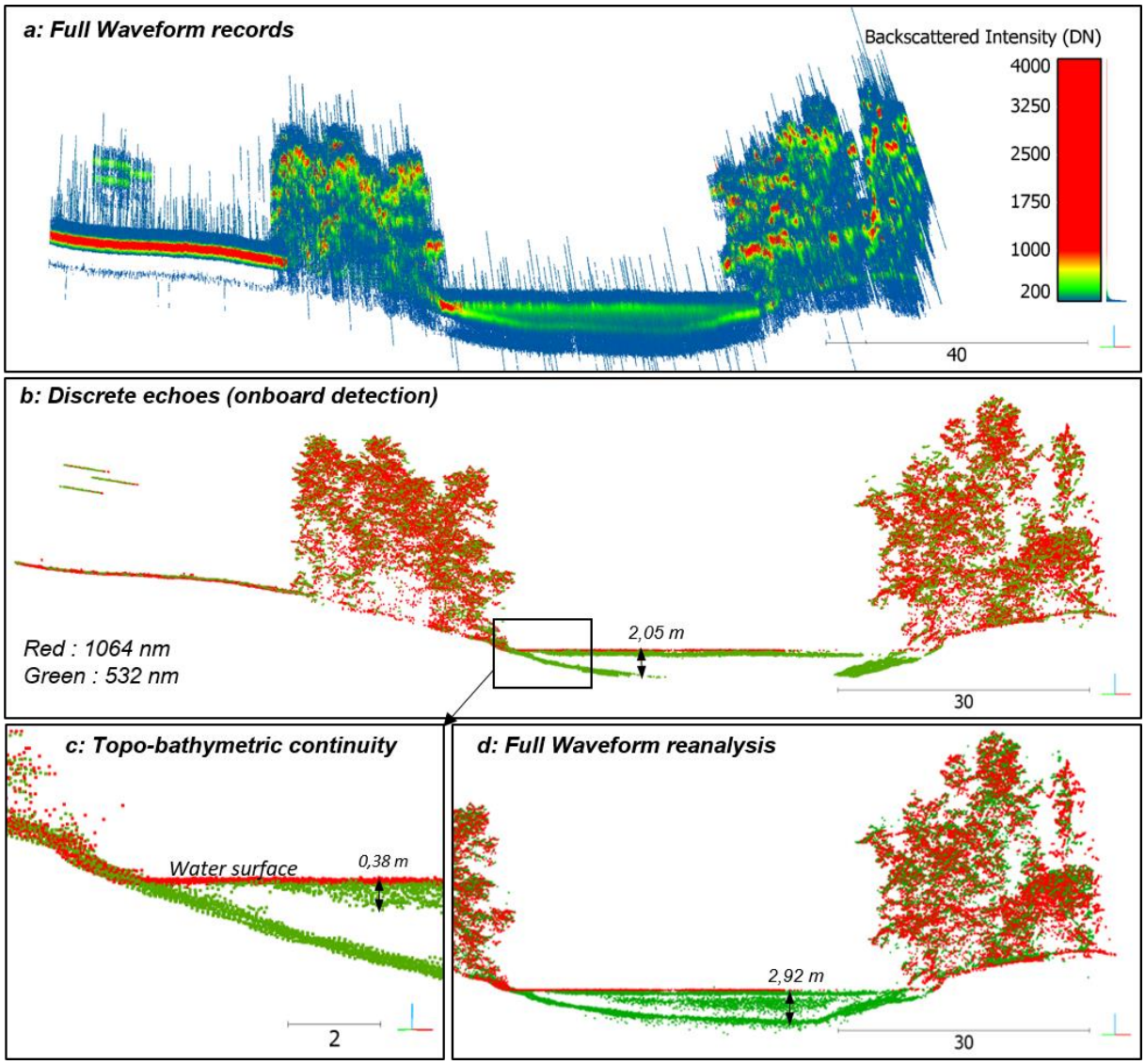

Figure 4: Cross-section on the River Ain illustrating: (a) the backscattered energy as recorded by the full-waveform records for each shot; (b) the discrete echoes recorded during the flight; (c) a detail of the topo-bathymetric transition showing the systematic offset of green surface echoes with respect to the true water surface documented by the 1064 nm channel; and (d) the reanalysis of the full waveform after the survey to recover weaker echoes, albeit with a larger uncertainty and stronger noise for the deepest ones, related to the simplistic approach used to detect echo (simple local maxima detection).

If we now focus on the issue of maximum depth detection, after travelling back and forth through the air/water interface and the water column, the bottom echo intensity theoretically obeys the following relationship (Abdallah et al., 2012; Cossio et al., 2009):

$$I_b = \frac{A_{sensor}}{l^2}(1 - L_s)^2 R_b exp\left(-\frac{2K_{d,532\,nm}D}{\cos\theta}\right) = I_{ref}\ exp\left(-\frac{2K_{d,532\,nm}D}{\cos\theta}\right), \qquad (1)$$

where I_b is the intensity of the bottom echo, D is depth, A_{sensor} contains various factors related to the instrument, which do not vary between surveys (e.g., emitted power, receiver area, gain), l is the along shot range to the water surface (we assume $l >> D$), L_s is the loss factor through the air/water interface, R_b is the bottom reflectivity at 532 nm and θ_w is the incidence angle in the water column. I_{ref} is the factor encompassing all other parameters but the water clarity effect. Because of the two-way travel through the water column, $K_{d,532\,nm}$ is multiplied by 2 in the exponential term, and the transmission loss is squared. As θ_w typically varies between 5 and 12° for the Titan sensor, we consider $cos\ \theta_w \sim 1$ as a first order approximation.

To evaluate the validity of eq. (1), we have selected three, 20-m-long river sections of the Ain and Rhone selected with uniform bed. A 2D kernel density smoothing with a standard deviation of 0.5 m was applied to the raw-intensity attribute of the point cloud in Cloudcompare in order to smooth out the fluctuations related to quantization of the backscattered signal near the limit of the detection level. Figure 5 shows that the exponential decay predicted between depth and echo intensity by eq. (1) is nearly perfectly verified in shallow rivers with only subtle deviations at very low intensity levels near the threshold of discrete echo detection.

Using eq. (1), we propose to estimate $K_{d,532\ nm}$ from the depth/intensity relationships by choosing sections for which $K_{d,532\ nm}$ and I_{ref} can be assumed spatially uniform and by considering only points on bed slope smaller than 5° to avoid pulse stretching effects (Abdallah et al., 2012). We have verified that the exponential decay of the intensity of discrete echoes with depth is observed in many rivers and coastal environments. This new calculation of $K_{d,532\ nm}$ is potentially more robust than estimates based on individual waveforms, given the difficulty in separating the 3 components of a bathymetric waveforms in shallow aquatic environments (Richter et al., 2017; Zhao et al., 2018). It has however a lower spatial resolution, and requires a uniform channel bed reflectance. For a given flight elevation, water turbidity and transmission loss, I_{ref} should be directly proportional to the bottom reflectivity. Knowing $K_{d,532\ nm}$ it is thus theoretically possible to normalize the intensity of bottom echoes from attenuation by depth, to generate intensity maps that should more directly reflect spatial variations in the bottom reflectivity, but also variations in bed slope due to the influence of pulse stretching on the peak echo intensity.

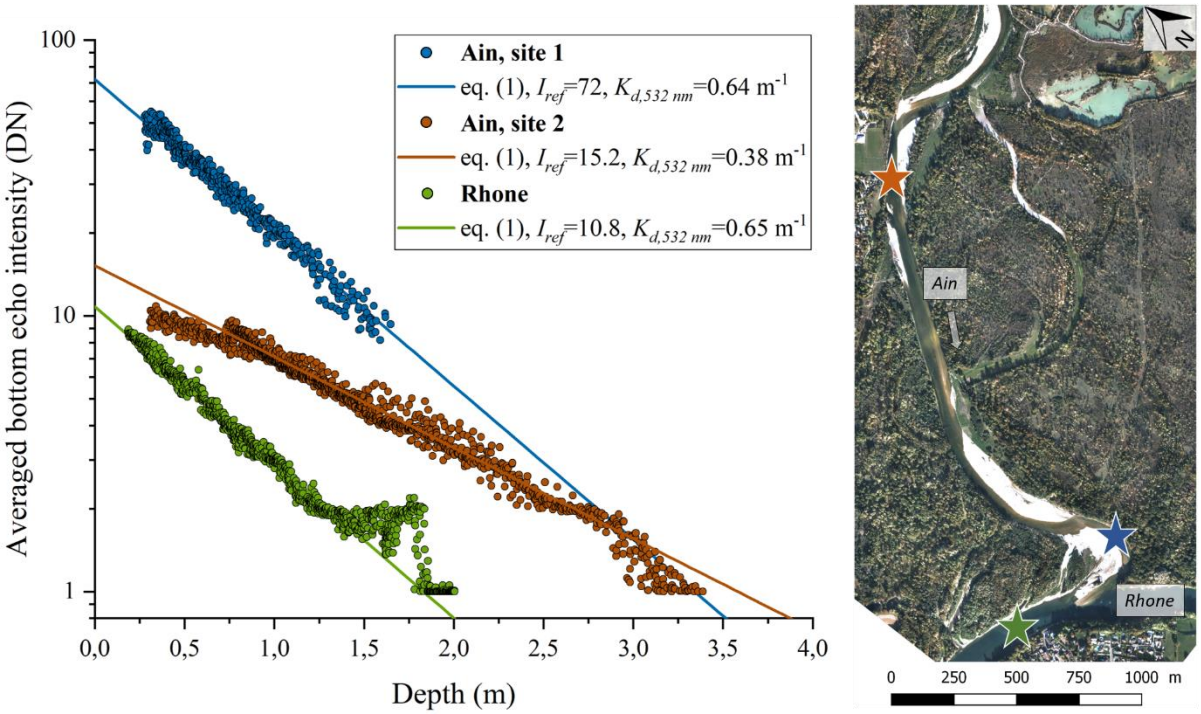

Figure 5 : Left: Intensity-depth relationship for the discrete echoes of the Titan DW when deployed over the River Ain on September 2016 near the confluence with the Rhône (see figure 1 for point clouds corresponding to this part of the survey). Each site is a 20-m-long reach corresponding to half the channel cross-section, removing the steep slope near channel banks. Data shown on the graphs correspond to point clouds subsampled with a minimum point distance of 0.5 m. This graph shows that the exponential decay of intensity with depth (eq. 1) is verified in shallow river environments. The back-calculated values of $K_{d,532\ nm}$ indicate that the Ain near its confluence (site 2) with the Rhone is more turbid than upstream (site 1). I_{ref} is expected to be directly proportional to bed reflectivity. Although the Ain has a more reflective bed than the Rhone, strong variations in reflectivity are observed within 2 km distance between site 1 and 2.

3.2 Results on maximum measurable depth and sensor comparison

If one considers that the maximum measurable depth D_{max} corresponds to a minimum detectable level of returned intensity I_{lim}, equation (1) can be rewritten as:

$$D_{max} = \frac{1}{2K_{d,532nm}} ln\left(\frac{A_s(1-L_s)^2 R_b}{I_{lim} l^2}\right) = \frac{1}{2K_{d,532nm}} ln\left(\frac{I_{ref}}{I_{lim}}\right). \quad (2)$$

Eq. (2) gives several quantitative insights into the controls of D_{max} (Legleiter et al., 2016). Apart from the sensor design contained in A_s and the signal-processing techniques contained in I_{lim}, D_{max} are inversely proportional to $K_{d,532nm}$ and increase as the logarithm of bottom reflectivity. Our work on French rivers without aquatic vegetation has shown that D_{max} varies between 1.6 to 5.6 m for discrete echoes. A preliminary analysis of $K_{d,532\ nm}$ and I_{ref} by intensity-depth relationships in those rivers led to $K_{d,532\ nm}$ varying between 0.3 and 1.1 m^{-1}, and I_{ref} varying between 10 and 100 (e.g., Figure 4). Using eq. (2), these data show that $K_{d,532\ nm}$ is the dominant environmental factor controlling D_{max} (~ 300 % variation), but that I_{ref} variations, that we interpret as bottom reflectivity variations, are almost as important (~ 200 % variation). Obviously, $K_{d,532nm}$ can be much larger than 1 m^{-1} in very turbid rivers, or during flood or post-flood conditions, but there would be little interest in surveying a river in that case. For comparison, data from coastal surveys at similar AGL in clear water and over bright sand, yield values of I_{ref} up to 200 and $K_{d,532\ nm}$ down to 0.1 m^{-1}, with D_{max} up to 11-12 m. This shows that in general, fluvial ALTB has a lower D_{max} than in coastal environments, and is thus more challenging due to a combination of lower-bed reflectivity and higher turbidity.

Comparing the actual performance of various sensors in fluvial environments is difficult as tests never occur with the same environmental parameters, or these parameters, in particular bottom reflectivity and $K_{d,532nm}$, are not known. Surveys on the same river but at a different period do not allow the comparison of sensor performance given the temporal fluctuations in turbidity and bed state. Manufacturers generally state the expected D_{max} of their sensor as a multiple of the inverse of the diffuse attenuation coefficient as in eq. (2) and specifying the bed reflectivity used for the calculation. For the Teledyne Optech Titan, D_{max}=1.5/$K_{d,532\ nm}$ with R_b=0.2. The Leica Chiroptera II is given for D_{max}=2.3/$K_{d,532nm}$ with R_b=0.15, and should thus provide deeper depth capability than the Titan. Note however, that these theoretical performances are given for $K_{d,\ 532nm}$ < 0.3 m^{-1} which in practice are rarely met in rivers we have surveyed in France. The Riegl sensors are given in terms of multiple of Secchi depth (e.g., 1.5 SDD for the RIEGL VQ-880G) and for R_b>0.8, which makes comparing with other sensors very difficult as the Secchi depth is not an inherent optical property of water, and the chosen R_b seems hardly representative of river environments. Few studies have systematically explored the maximum depth reachable in various river systems, and not all studies report D_{max}. Values ranging from 0.7 to 3.5 m have been reported for the Optech Aquarius system in rivers (Fernandez-Diaz et al., 2014; Legleiter et al., 2016). These authors have highlighted the likely role of spatially variable bottom reflectivity in modulating D_{max} on top of the strong impact of water turbidity.

3.3 Depth uncertainty and detail resolving capability

Depth accuracy and precision are critical to a variety of applications, in particular the measurement of erosion and sedimentation from repeat surveys. From a theoretical point of view, the physics of laser interaction with the ground is similar in air or water, and thus the same level of uncertainty is expected. With modern ALS sensors and state-of-the-art GPS/IMU flown at an AGL of 400 m, a vertical error magnitude of 5 cm and an horizontal error of 20 cm would be expected on flat surfaces (Passalacqua et al., 2015). Yet, the error budget of bathymetric river echo must include the water surface detection and refraction correction, as well as uncertainty on the peak detection method when dealing with full waveform data (Pan et al., 2015). Echo detection becomes critical in non-optimal conditions such as low water depth with overlapping surface and bottom echoes (figure 3), or where water turbidity results in weak echoes. Pan and co-authors (2015) highlights the strong influence of waveform echo processing on the accuracy and precision of depth measurement for the Optech Aquarius system. In the best conditions, the mean accuracy is of the order of 2 cm, with a precision of 13 cm (1std deviation). However, this result degrades in turbid water. Discrete echoes are nearly as accurate as the best full waveform processing method. Recent results with EEARL-B compared to GPS surveys shows RMSE varying between 10 and 20 cm with no dependence on depth (Daniele et al., 2018). Mandlburger and co-authors (2015) measured a precision of 4 cm (1 std) in shallow bathymetry.

The range of error reported may reflect sensor and processing methods, but it may also reflect the different nature of the validation data, especially in rivers with a rough bed. Single beam sonar or ADCP are often used as a reference bathymetry. However, their narrow beamwidth angle θ (e.g., < 1°) will sample the bed over an area generally much smaller than 10 cm at shallow depths (< 2 m). On the contrary, the sampling of the bed by the laser will typically average the elevation over a surface of at least 20-30 cm. As such, even if the measurements were made on exactly the same horizontal position, the depth measured would be different owing to the different sampling of the rough bed. The same sampling bias may exist when comparing bed elevation with GPS pole measurements, in particular in sloping areas such as banks (Daniele et al., 2018). This highlights the need to evaluate the accuracy of ALTB on flat smooth channel bottoms and properly account for the sampling area of each technique.

The capability of ALTB to resolve fine details on the channel bed depends on the point density, the scan pattern, and the laser spot size. The high PRF of the latest generation of ALTB results in point densities of 15 pts/m² in one pass. The point spacing is generally inhomogeneous, owing to the scanning pattern. Yet, the flight line overlap will typically densify the point cloud to 20-30 pts/m², such that the limit in the effective resolution of the data is in general the laser spot size. For the Titan flown at 400 m, the spot size averages the bed over 0.25-0.3 m at shallow depth and in clear water conditions. Consequently, details larger than 0.25 m horizontal scale should be captured by ALTB. Below this scale, roughness features are likely translating into higher point cloud noise, however their measurement is biased by the smoothing effect of the laser spot size. A critical aspect to evaluate roughness features is the vertical precision of bathymetric points. Figure 4.8 shows details of the refraction-corrected, raw point cloud corresponding to a reach of the Ain. Large boulders and a tree trunk are clearly visible and measurable. The roughness measured as the standard deviation of the elevation over a 1 m circle is as low as 6 mm in flat smooth surfaces, illustrating excellent precision characteristics of the sensor.

3.4 Surveyable rivers and survey strategy

Currently no way exists to be 100 % certain that a river is fully surveyable with ALTB given the difficulty in knowing $K_{d,532nm}$ and I_{ref} beforehand. However, our experience in deploying the Titan DW sensor over various rivers in France has shown that the suitability of a river for ALTB and the optimal survey season depends on 3 constraints (figure 6):

- the first one is hydrological and imposes to acquire data with the lowest mineral and organic turbidity conditions and the lowest water level. A rule of thumb is that, if the channel bed is largely not visible during the low-flow season either due to high turbidity levels or depth greater than 4-5 m, then the likelihood of a successful bathymetric cover decreases greatly.
- The second one relates to the biological component: it imposes to acquire data with leaf-off conditions for riparian vegetation and the lowest aquatic vegetation cover possible. This includes periphyton cover on the channel bed. Similarly, summer phytoplankton bloom in rivers can generate a high level of organic turbidity. In general, these penalizing effects are typical of a low energy river with very infrequent bedload transport.
- The third constraint relates to weather conditions that will alter the likelihood of meeting optimal conjunction of low water level and good flight conditions.

A final critical aspect governing the likelihood of complete bathymetric cover is the depth distribution near D_{river}. Straight rivers with a flat bottom can be largely unsurveyable if D_{river} is only slightly above D_{max} on the day of the survey. However, meandering rivers, or rivers with actively migrating bars (alternate bars, braided rivers) will have a broader range of depth, ensuring that if D_{river} is only marginally larger than D_{max}, a large part of the channel bed could still be surveyed. Interpolation or complementary surveys by sonar would be enough to cover the missing data. In these type of rivers, two different strategies can be followed depending on D_{river} during the low flow conditions: if D_{river} > 3 m, the strategy will always be to fly during the lowest flow conditions, whatever the state of the riparian vegetation (figure 6). If riparian vegetation is nonetheless prominent, the point density and bathymetric

cover will be reduced near and on banks. If D_{river} < 3 m and the riparian vegetation is significant, the survey should occur during early spring or late autumn conditions when the river is not necessarily at its lowest level, but where leaf-off conditions are preferable to maximize the visibility of the channel.

As D_{river} > 3 m for the Ain during the lowest flow conditions, we choose a summer survey. D_{max} with discrete echoes was close to 4 m, and a post-processing of the bathymetric waveforms to detect weaker echoes resulted in a gain of about 25% in depth (up to 5 m). This offered a complete bathymetric cover of the downstream 30 km of the river where the channel bed is highly mobile with riffle/run/pool structures. The bed cover was more limited in the upstream part where the river is confined, with a flatter and deeper bed. The very high shot density resulting from the combination of the two lasers (> 40 shots/m² on a single pass), resulted in the floodplain ground being accurately sampled despite leaf-on conditions.

Low-energy rivers with dense riparian and aquatic vegetation are challenging and not necessarily suitable for ALTB despite very shallow and clear water. Even if surveyed during low-flow conditions in summer with D_{river} < 1.5 m, screening by riparian vegetation, aquatic vegetation and duckweed can result in poor bathymetric cover. For these systems, it is essential to fly between the end of autumn and early spring in leaf off conditions and reduced aquatic vegetation cover. But flying opportunities reduces drastically and even with leaf off conditions, low energy rivers with very infrequent bedload transport tend to have very dark bed with low reflectivity, very likely related to the development of periphyton (Legleiter et al., 2016). A high degree of uncertainty thus occurs on the final bathymetric cover achievable on these type of fluvial environments.

We conclude that energetic rivers with active bedload sediment transport, mobile bars, reduced aquatic vegetation and periphyton cover, and high water clarity ($K_{d,532\ nm}$ < 0.3 m^{-1}) are surveyable with the Titan DW sensor using existing full waveform-processing techniques down to 5-6 m. As bed mobility decreases, or turbidity increases or the biological component starts to be dominant, the maximum flow depth decreases down to values ranging from 0.5 to 2 m on channel bed without aquatic vegetation cover.

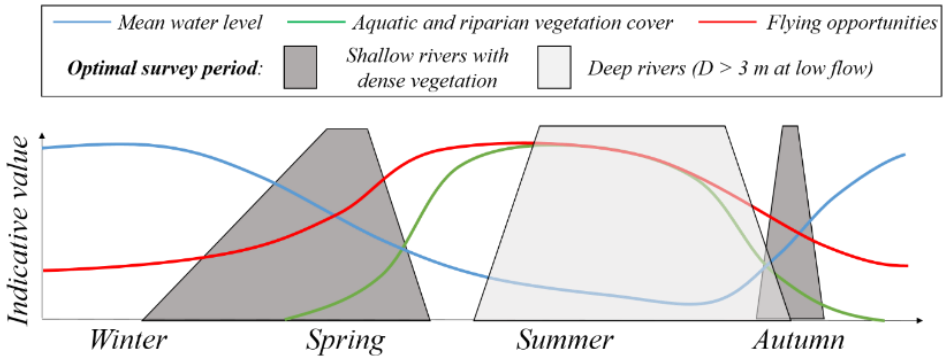

Figure 6: Optimal survey period as a function of the 3 main constraints governing topo-bathymetric airborne lidar acquisition in fluvial environments. For deep rivers, the main limiting factor is the water level, whatever the vegetation constraints. For shallow rivers (< 1-2 m in low flow) with high aquatic vegetation or riparian cover, the optimal survey seasons are around spring and autumn, but with reduced chance of success due to more frequent adverse flying conditions, increased flood frequency and higher turbidity levels. For snowmelt controlled rivers, the optimal survey season can be winter.

4. Data processing

4.1 Water surface detection, bathymetric classification and refraction correction

Beyond the standard post-processing of airborne lidar data (Glennie et al., 2013; Vosselman & Maas, 2010), the 532 nm points below water require a geometric correction to account for the refraction of the laser beam and reduction of the light celerity at the air/water interface. In practice, for incidence angles

ranging from 7 to 20° the apparent depth is larger than the true depth by a factor varying from 0.74 to 0.71. At a 2 m depth, the horizontal correction, will range from 10 to 40 cm depending on the incidence angle, and can be up to 1 m at 5 m depth. Given the very low slope of rivers and the small amplitude of surface waves, assuming a locally horizontal water surface is acceptable. In that case the correction in X,Y and Z can exactly be computed given the knowledge of the laser shot 3D vector obtained from the instrument trajectory, the bathymetric point apparent position, and the water surface position (e.g., Guenther et al., 2000).

Compared to coastal environments where the water elevation can be assumed horizontal on a given flight line, the detection of the water surface and of the 532nm points requiring correction is by far the most challenging phase in large-scale, topo-bathymetric surveys of rivers. This arises from the hydraulic slope of the river, the complexity of a river's boundaries (e.g., sinuosity, multiple channels, vegetation), the large water elevation fluctuations near dams or chutes, and the need to detect the water surface of nearby aquatic bodies (e.g., lakes, ponds, abandoned channels, ditches). These non-fluvial features are actually essential to study floodplain hydrology and connectivity. Another challenge specific to fluvial environments relates to the non-uniform sampling of the water surface by the 1064 nm laser (Höfle et al., 2009) due to specular reflection on low-velocity, flat water. It is thus not possible to assume that the water surface is always sampled by the 1064 nm channel just above any given 532nm point. It is also not possible to assume that the lowest point of the 532 nm point cloud is the bathymetry in a river, given that the bed may not have been sampled (i.e., $D_{river} > D_{max}$). Previous surveys dealing with small reaches (< 1 km) have used a combination of manual digitizing of the river axis (Mandlburger et al., 2015), followed by automated detection of the water surface, or digitization of the channel boundary followed by subsequent extraction of water elevation from the 1064 nm channel (Legleiter et al., 2016; Pan et al., 2015). Any manual intervention on the data to initially identify the water surface, however, is not possible for large scale surveys (> 1 km), and is in general not desirable as the operator might miss small inundated areas below the canopy. Although sensor manufacturers generally provid- a solution to automatically classify surface echoes and bottom echoes in coastal or lake environments (and perform subsequent refraction correction), we are not aware of tests assessing the performance of these solutions over complex fluvial environments.

To illustrate the level of automatic processing that can be achieved on large scale surveys, we briefly show results from an algorithm of automatic bathymetric classification that we have developed working on raw 1064 and 532 nm point clouds. This approach does not use the waveform signal, but rather uses the difference in water depth penetration of the 1064 nm and 532 nm channels, and the flat nature of the water surface measured by the 1064 nm. It leverages the command line function of the open source software CloudCompare (EDF R&D, 2011) for scripting efficient 532 nm/1064 nm point cloud comparison and 3D morphological operations (roughness, slope, point density, lowest point extraction). It can process several billion points to create a low-resolution (2 m point spacing) classification of the water surface echoes on the 1064 nm channel and of bathymetric points in the 532 nm channel in less than one hour on a 48 cpu server. The low-resolution water surface composed of only a few thousand points can then be checked manually for quality control, and is either densified with neighboring 1064 nm echoes, interpolated if the point density is too low, or directly used in subsequent calculations. The resulting uncorrected depth map can be converted to an approximate depth map by multiplying by a factor of 0.73. This serves as a quick estimate of the bathymetric coverage used to plan additional sonar surveys in deep areas, but cannot be considered a final product as the horizontal correction of refraction must be accounted for.

The final water surface 1064 nm point cloud is the key ingredient to a subsequent accurate refraction correction and high-resolution classification of the 532 nm and 1064 nm point clouds. In particular, 532 nm points locally above the nearest water surface point of the 1064 nm are classified as land and subsequently classified with traditional topographic airborne lidar techniques (Vosselman & Maas, 2010). The position of 532nm points below the nearest 1064 nm water surface point is corrected for

refraction and laser celerity change, and then classified as bottom echoes, water surface or water column echoes using a combination of depth/intensity analysis (figure 5) and morphological analysis.

Figure 7 shows the result of a typical water surface classification on the lowest 13 km of the River Ain survey. Beyond accurately detecting the main river and large open water bodies such as lakes, the algorithm is able to capture abandoned channels largely screened by the tree canopy, small ponds, and swimming pools. This offers new perspectives to study the hydrological connectivity of floodplains and rivers, as well as hydrology under forest canopies.

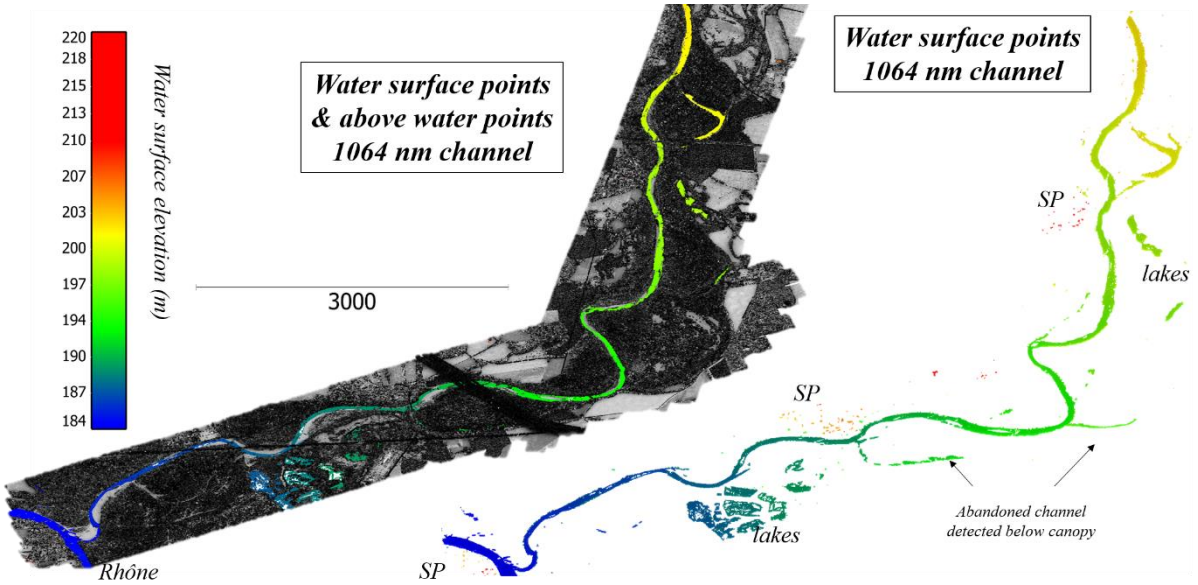

Figure 7: Example of automatic detection of the water surface using the 1064 nm wavelength. The main channel surface is detected, but also abandoned channels below canopy, lakes and swimming pools (SP) in the villages bordering the river. The 1064 nm water-surface point cloud is the key element for an accurate land/water classification of the 532 nm point cloud, as well as the refraction correction of bathymetric points.

4.2 Full-waveform analysis

Compared to point-cloud processing, FWF processing is more challenging as few software packages exist to visualize and process it, and the volume of data is typically 10 times larger than compressed point clouds. The open source software CloudCompare (EDF R&D, 2011) can now handle FWF visualization and processing thanks to developments funded by our team (Figure 4), but many challenges exist to overcome the use of FWF routinely. While FWF processing is not mandatory if discrete echoes are deep enough, it can potentially help in recovering weaker echoes (Figure 3), increase accuracy, inform on water column turbidity (Pan et al., 2015; Richter et al., 2017) and bottom characteristics. Similar to topographic airborne lidar FWF processing (e.g., Mallet & Bretar, 2009), many different peak extraction techniques have been developed with no consensus yet on the best one for bathymetric waveform processing (Pan et al., 2015; Saylam et al., 2017). Preliminary attempts at retrieving $K_{d,532nm}$ from single waveform shots to map spatial variations of river-water turbidity have had mixed results due to the overlap of surface echoes, water column backscatter, and bottom echoes in shallow environments (Richter et al., 2017). As for point clouds, waveforms should also be corrected for refraction. FWF can be studied for a single shot, or aggregated spatially into an equivalent vertical waveform called an orthowaveform (Pan et al., 2016; Wu et al., 2012). Orthowaveforms have the benefit of transforming the waveform 3D field, into a grid of waveform signal with regular horizontal spacing that facilitates the comparison with hyperspectral or multispectral imaging (Pan et al., 2016).

5. Applications in fluvial geomorphology

The fluvial geomorphology community has cautiously observed the advent of ALTB, and only a handful of ALTB surveys occur that cover more than a few kilometers of rivers (McKean et al., 2009). As such,

ALTB has not yet moved from the realm of a promising remote sensing technique to a day-to-day survey technique for geomorphological analysis, both in the academic and private sector. In the following section, we summarize the existing applications of ALTB and illustrate scientific opportunities. First, we summarize the main data available at hand for the fluvial geomorphologist following a successful survey using the latest generation of ALTB sensors:

- A continuous topo-bathymetric survey with point density of the order of 10 -20 pts/m², accurate to within 10 cm under water and 5 cm above water. Laser spot size sets the capacity to resolve details, which for the Titan is of the order of 20-30 cm.
- A water surface known at +-2 cm with the 1064 nm channel, albeit with incomplete spatial sampling.
- A 3D characterization of riparian vegetation potentially with bi-spectral intensity information.
- Relationships between depth and intensity that are quantitatively related to the water column optical properties and variations in bottom reflectance (eq. 1).
- An optional full-waveform record for each shot with elements of the records that depend on the physical characteristics of the environment (turbidity, bottom reflectance, water surface roughness)
- Optional high resolution multispectral or hyperspectral orthoimagery (Legleiter et al., 2016)
- All this acquired over several tens of kilometers.

These data can be augmented with in situ measurements. Water discharge should be measured on the day of the survey in as many points as deemed necessary given the number of confluences. The optical properties of the water should be measured in various locations, with methods ranging from simple SDD measurements to more accurate inherent or apparent optical properties of the water in the 532 nm wavelength, as well as bottom reflectance (Legleiter et al., 2016). Water could also be sampled in various spots for suspended sediment concentration measurement.

5.1 Multi-scale high resolution fluvial geomorphology

The first straightforward application of topo-bathymetric lidar is the 3D analysis of channel geometry at various scales. Mckean and co-authors (2009a, 2008) have pioneered this approach and have illustrated a large range of applications using EAARL data, ranging from characterizing morphological units (e.g., pools, riffle) to cross-section characteristics, longitudinal profile (e.g., slope, width variation) and the relationship between floodplains and channels (e.g., connectivity). The advent of sensors creating denser point clouds (> 20 pts/m²) with very low positioning noise also offers the possibility to explore below the 1 m² scale of EAARL data, in order to address spatial variation in bed roughness (Figure 8). Quantifying this variation is useful when exploring the heterogeneity of channel-bed conditions with relevance to friction modelling and in-stream, meso-habitat prediction. The ability to resolve details of the channel bed must be carefully addressed by accounting for the point cloud pattern, the bathymetric precision, the laser spot size, and the accuracy of flight line adjustment. As shown on sample data of the Ain (Figure 8), sensors such as the Titan are able to resolve individual boulders and tree trunks down to approximately 20-30 cm. The ability to resolve details decreases with depth and river turbidity as diffusion increases the laser-spot size on the bed. In the case of the River Ain, bed roughness measured over 1 m is as low as 6 mm on smooth bathymetric surfaces under 2 m of water, but can increase up to 10 cm in cobble-bed areas.

Modern topo-bathymetric surveys can easily address morphological characteristics over about 5 to 6 orders of magnitude (0.2 to 100000 m) both below and above water. This is unprecedented. Arguably, the full potential of ALTB for geomorphological analysis has not yet been realized. As for topographic lidar (Passalacqua et al., 2015), synoptic, high resolution high precision 3D topo-bathymetry requires a change in paradigm to describe rivers beyond the traditional planform or cross-sectional view inherited from coarser survey approaches. The 3D continuous nature of the river and its relationship with the floodplain and riparian vegetation must now be included.

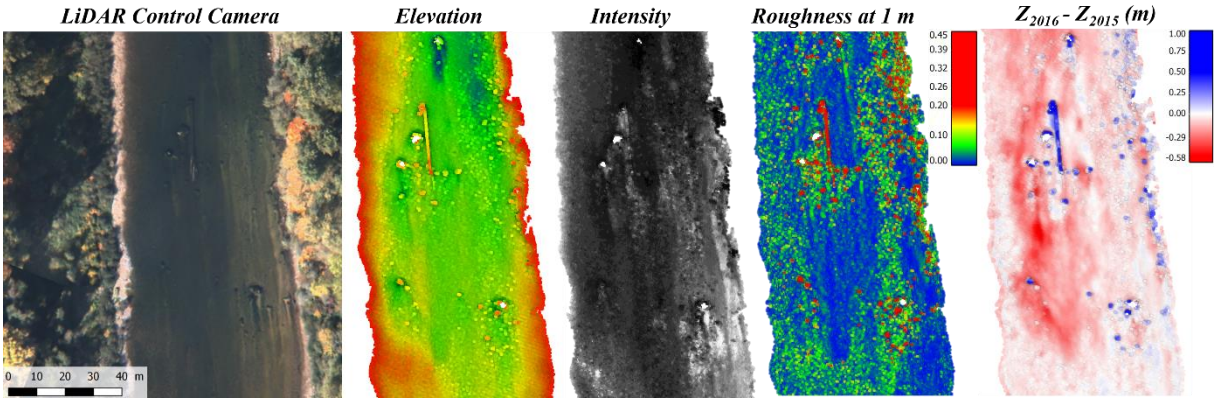

Figure 8: Illustration of resolution and accuracy capabilities of the latest generation topo-bathymetric sensors (Optech Titan DW). Excerpt of the 2016 Ain raw survey point cloud illustrating the capability to detect tree trunks and large boulders in the river bed as well as variable bed roughness (standard deviation of elevation measured over a 1 m sphere diameter, computed directly on the 3D point cloud with Cloudcompare). Note that the minimum roughness is 6 mm in the smoothest parts of the bed, illustrating excellent ranging noise capabilities under 2 m water depth. Topographic change between September 2016 and July 2015 measured with M3C2 algorithm at 1 m scale directly on point clouds (Lague et al., 2013), and showing the deposition of a tree trunk and several individual boulders of metric size, as well as erosion downstream of the tree trunk.

5.2 Coupling with 2D-3D hydraulic modelling

Given that ALTB surveys are performed during low flows, the water-surface slope and the flow depth extracted from these data are hardly representative of the large range of discharges experienced by the river. Applying computational models of fluid dynamics to fluvial topo-bathymetric data is thus a quasi-mandatory approach to fully harness the potential of ALTB (Mandlburger et al., 2015; McKean et al., 2009, 2014). Such models can be used to predict flow velocities, water depth, and shear stresses occurring during discharges large enough to be relevant to processes such as bedload transport, channel-bank erosion, boulder mobility, and floodplain/channel connectivity. 2D hydraulic models have been used for fluvial habitat mapping over small reaches (Crowder & Diplas, 2000; Mandlburger et al., 2015), but the challenge now lies in applying such models over very long reaches and high resolution. It is beyond the scope of this chapter to offer a complete review of CFD modelling capabilities and limits. Figure 9 illustrates potential applications of a 2D hydraulic model resolving the vertically averaged St-Venant equations without inertia applied on a 1 m topo-bathymetric DEM of the Ain over a 4 km long reach (Davy et al., 2017). This model is fast and can thus be used to explore the impact of varying discharge or friction coefficient. For instance, an average friction coefficient was calibrated by minimizing the difference between the predicted water-surface elevation and the measured water-surface elevation given the knowledge of the discharge at the time of the survey. Exploring the spatial variations of the residuals can then offer insights into the quality of the model prediction.

Beyond model calibration, the inundation pattern, flow depth, velocities, and shear stress can be predicted in the river and the floodplain for a large range of discharges (Figure 9). From this set of high-resolution inundation maps obtained for various discharges, several applications can be envisioned. Here we illustrate a few possibilities. First, at any given channel location, the hydraulic geometry of the channel can be computed in the form of rating curves of a hydraulic variable (e.g., depth, velocity, hydraulic slope) versus discharge. Second, inundation patterns and flow velocities can be predicted for very large discharges in the context of flood-hazard prediction. Third, at any point in the floodplain, the classified vegetation cover obtained from the above ground ALTB data can be compared to hydrological forcings such as inundation frequency or flow velocity during large flood events. Fourth, for any relevant discharge, such as the bankfull discharge, the morphological units can be mapped as a function of a combination of geometrical characteristics and flow velocities (Mandlburger et al., 2015). These are only a handful of possibilities that CFD modelling coupled with ALTB is likely to offer in the coming years for fluvial geomorphology applications.

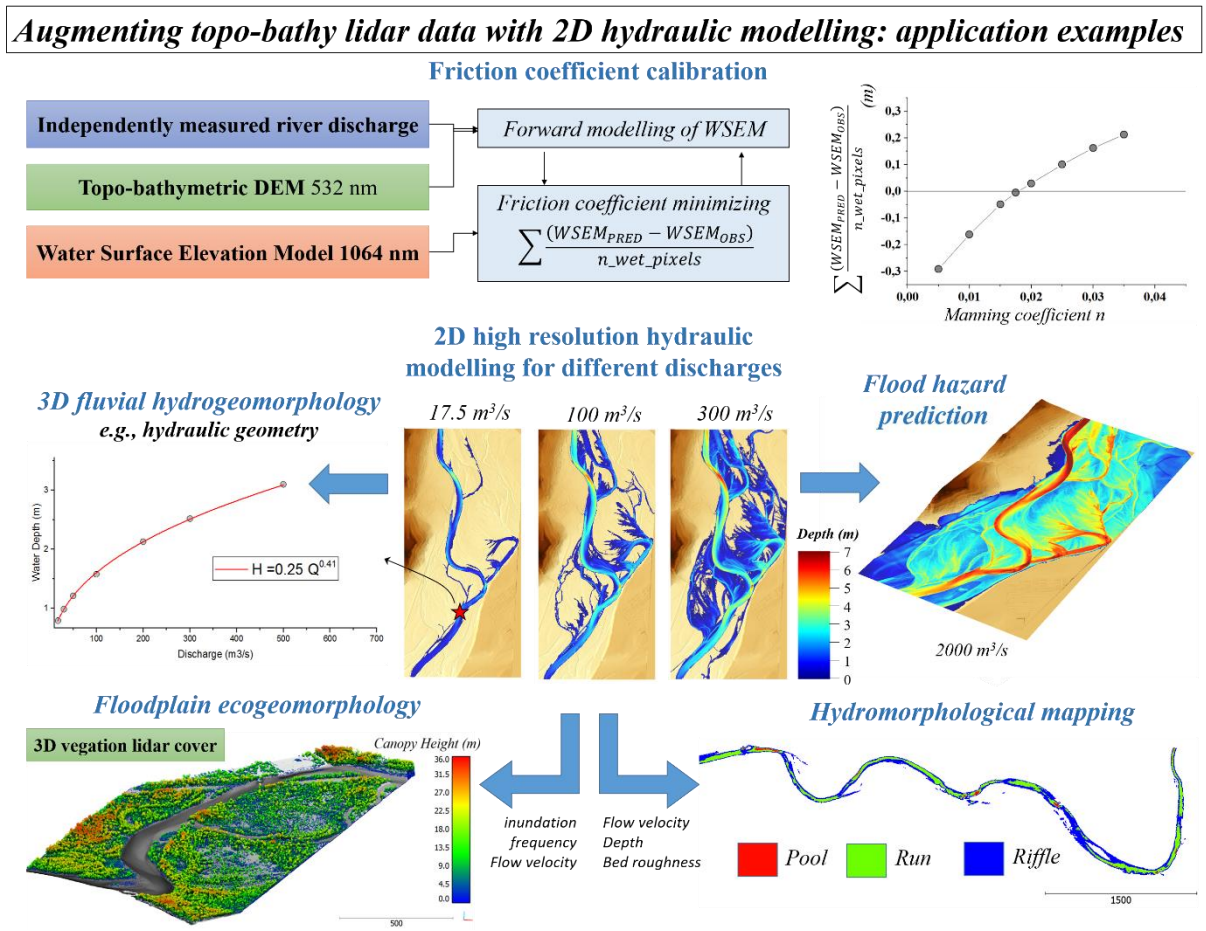

Figure 9: Application examples of 2D high-resolution hydraulic modelling applied on large scale (4 km) topo-bathymetric survey. A 1-m continuous topo-bathymetric DEM of a 4 km long reach of the Ain is used as a boundary condition to the hydrodynamic component of the EROS model that solves the vertically averaged St-Venant equations without the inertial term (Davy et al., 2017). Flow direction is from top to bottom.

5.3 Synoptic channel morphodynamics and sediment budget

As for many high resolution topographic applications (Passalacqua et al., 2015), repeat ALTB surveys offer the potential of exploring channel morphodynamics in a completely new way (Mandlburger et al., 2015; McKean et al., 2009). The lack of bathymetric information using airborne or ground-based lidar or photogrammetry has always resulted in large uncertainties in measuring erosion and sedimentation patterns in rivers, as well as constructing sediment budgets. Getting repeat surveys of inundated areas where most of bedload sediment transport occurs is essential for improving our understanding of how rivers evolve, and in particular the impact of extreme events over a broad range of scales.

A critical aspect for repeat surveying is the level of change detection that is achievable with ALTB. Various approaches are possible to develop an error budget for airborne-lidar, point-cloud comparison (e.g., Passalacqua et al., 2015). Three sources of uncertainty should be considered: (i) the co-registration error of the 2 surveys that must be evaluated with fixed reference surfaces and can be assumed either uniform (Wagner et al., 2017) or spatially variable (Joerg et al., 2012); (ii) the position uncertainty that may be different on topography and bathymetry; (iii) the surface roughness which introduces uncertainty in point-cloud comparison due to differences in sampling between the surveys (Lague et al., 2013). In the simplest approach possible, one can consider a spatially uniform registration error $\sigma_{\overline{reg}}$, and a spatially variable error made of a combination of a position uncertainty Z_{err} and point-cloud roughness σ_z evaluated over the spatial scale at which vertical averaging occurs. Point-cloud roughness results both from surface roughness but also errors in flight-line adjustment in overlapping areas, ranging noise, or classification errors (Wagner et al., 2017). To evaluate the standard error of the vertical topographic

difference with typical Titan topo-bathymetric surveys, we assume that the roughness component is uncorrelated between the two surveys and that the survey have the same densities, position uncertainty and point-cloud roughness. In that case, the standard error is given by:

$$SE = \sqrt{\sigma_{\overline{reg}}{}^2 + \frac{Z_{err,1}^2 + \sigma_{z,1}^2}{n_1} + \frac{Z_{err,2}^2 + \sigma_{z,2}^2}{n_2}} \qquad (3),$$

where n_1 is the number of points contained in the surface used to compute the average position and the roughness $\sigma_{z,1}$ of the first (resp. second) survey, and n_2 and $\sigma_{z,2}$ are the equivalent values for the second survey. Here we assume that Z_{err}, σ_z and n are identical during the two surveys, but these values can easily be calculated from point clouds to have a spatially variable standard error (e.g., Wagner et al., 2017). In the Ain near the confluence with the Rhone (Figure 10), $\sigma_{\overline{reg}}$ = 2.58 cm (measured as the standard deviation of the M3C2 difference at 1 m between 2015 and 2016 of 10000 points on roads). As shown in Figure 8, point cloud roughness measured at 1 m scale varies from 0.6 cm to more than 30 cm near large boulders, while the point density is typically 20 pts/m². If we assume conservatively that Z_{err} = 10 cm under water and Z_{err} = 5 cm above water, the combined standard error under water varies from (Table 2) 4.38 cm in low roughness areas, to 8.31 cm in high roughness areas. Because of the high point density, the standard error is not very different under and above water for a single laser. But the doubling of point density by combining the 532 nm and 1064 nm above water further reduces the influence of position error and point-cloud roughness, such that the registration error is the dominant source of uncertainty in low-roughness zones.

Table 2: Standard errors corresponding to a vertical topographic change measured over a 0.5 averaging radius for point densities typical of the Titan DW (20 pts/m²), and bed roughness typical of the Ain survey (see fig. 8). Calculation using eq. (3) and registration error of 2.58 cm

	Low roughness σ_z = 0.6 cm, n= 16	**High roughness σ_z = 20 cm, n= 16**	**Low roughness, double ppm σ_z = 0.6 cm, n= 32**
Bathymetry, Z_{err} = 10 cm	4.38 cm	8.31 cm	3.60 cm*
Topography, Z_{err} = 5 cm	3.13 cm	7.73 cm	2.87 cm

*: if one would double point density by imposing a 50 % flight line overlap

Table 2 shows that the standard error is of the order of 4 to 8 cm with the Optech Titan. When considering the topographic change measured on the Ain near the Rhone confluence (figures 8, 10), these predictions show that most of the change is largely above the standard error. In the downstream section (Figure 10), the dominant change is related to channel lateral mobility in the sinuous parts. Finer details can be resolved, such as boulder movement (Figure 8), deposition of tree trunks, and bed accretion/erosion on the order of a few decimeters in relation to the wake developed by roughness features. These results illustrate the ability of repeat ALTB surveys to precisely document channel morphodynamics. In this context, the high shot density of modern ALTB not only offers the capability of resolving finer details of the channel bed, but it contributes to dividing by a factor 4 to 5 the standard error associated with stochastic components of the error budget compared to the early ALTB systems.

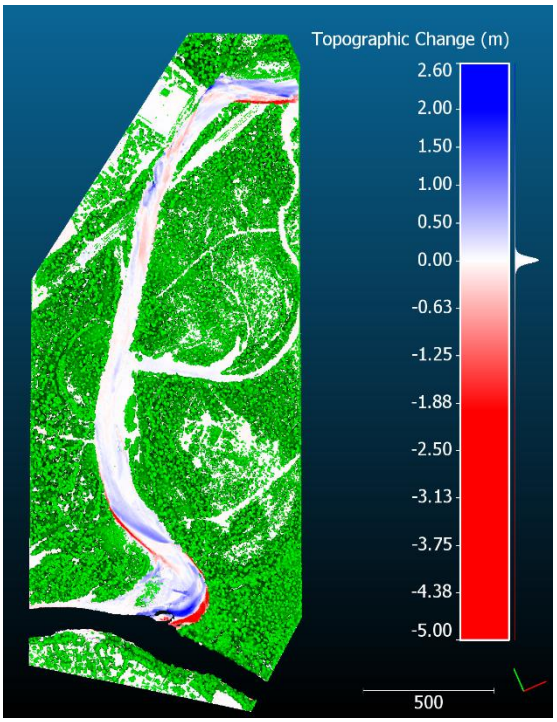

Figure 10: Topographic change of the Ain river between September 2016 and July 2015, measured directly on topo-bathymetric point clouds after vegetation classification as the mean vertical difference averaged over a 0.5 m radius circle (M3C2 algorithm, Lague et al., 2013). The dominant signal is the lateral mobility of the Ain River, driving accretion inside bends and bank erosion outside. The vegetation cover of the 2016 survey is shown for reference. No data are available on the Rhone, as the turbidity and water levels during the 2015 survey resulted in the absence of bathymetric measurement.

6. Conclusions and remaining challenges

Topo-bathymetric lidar can now be considered an operational technique to obtain synoptic, 3D high-resolution and high-accuracy surveys of rivers characterized by clear water and bed, mobile sediment with reduced aquatic vegetation cover. Depth down to 5 m can be reached in the best conditions with accuracies better than 10 cm. The continuous nature of the topography and bathymetry makes it suitable for a wide range of geomorphological applications, including erosion/sedimentation mapping with repeat surveys. As sensors have now reached a good level of maturity, four challenges need to be addressed to predict the surveyability of any given river and turn the dense lidar point clouds into usable scientific datasets for geomorphological science:

6.1 A priori prediction of depth penetration and river bathymetric cover

Sensor deployment on a new river still suffers from some uncertainty on the maximum measurable depth D_{max}. Although the theory predicting D_{max} is well established (eq. 4.2) (Abdallah et al., 2012; Guenther, 1985), many of the physical parameters related to river environments are not known. This makes the a priori prediction of the extinction depth D_{max} difficult. No reason exists, however, for the range of $K_{d,532\ nm}$, R_b and L_s to be better constrained in the future for river environments through direct measurement of inherent optical properties and bottom reflectivity, discrete echoes, and full-waveform analysis as in Figure 4.3, or the use of multispectral/hyperspectral imagery (Legleiter & Fonstad, 2012). This will help in narrowing down the type of rivers for which ALTB is not suitable due to high turbidity or low bed reflectance before acquiring any data.

6.2 Automatic classification on massive lidar datasets

Fluvial environments can be considerably more challenging than coastal environments when it comes to the refraction correction of bathymetric echoes. Applications of ALTB over very long river corridors is still in its infancy and any kind of manual processing considerably increases the final cost of ALTB

data. Automated post-processing is thus mandatory. We have developed in-house techniques to process large datasets for accurate refraction correction, but a more systematic classification of fluvial features relevant to geomorphology is needed. This includes the automated identification of banks, pools, bars, dunes, dams, boulders, bridges, riparian vegetation, terraces, or any feature of fluvial environments that can be used to enrich the 3D description of data for scientific analysis. Biogeomorphological analysis is expected to benefit significantly from advanced classification methods able to capture species diversity in relation to geomorphologic features.

6.3 Full-waveform analysis in the context of fluvial environments

The analysis of full-waveform records can benefit from previous work done on coastal environments, but should also consider the specificity of shallow fluvial environments and topo-bathymetric sensors. In particular, the shallow depth makes the separability of surface echoes, water-column backscatter, and bottom reflection more complex. Progress in using FWF records as an actual signal from which physical characteristics of the water surface, column, and river bed can be inverted will depend on two elements: first, the development of new signal-processing methods to improve depth accuracy, deconvolve the effect of system-impulse response, and increase the detection of weak echoes to maximize the depth capability. Second, the acquisition of reference data sets in a variety of fluvial environments for which in situ measurements of optical properties, water turbidity, bottom reflectance, depth, and detailed analysis of water surface characteristics are precisely measured.

6.4 Large scale hydraulic modelling on topo-bathymetric data

As ALTB datasets progressively grow in size due to both larger surveys and better resolution, the need for large scale 2D and even 3D hydraulic modelling operating at a sub-meter resolution increases. Hydraulic modelling should be viewed as an essential data augmentation approach in the context of fluvial ALTB. Although topo-bathymetric data alleviate the traditional problem of defining the numerical model domain, based on a limited set of channel cross-sections, it remains however computationally too demanding to operate the current generation of 2D hydraulic models over very large scales (i.e., > 50 km) at sub-meter resolution. ALTB data also offer new opportunities to validate model prediction based on water-elevation prediction and inject spatially explicit, friction variations using 3D information such as bed roughness and riparian vegetation to improve modelling accuracy.

Acknowledgments

The Titan DW sensor, operated by the Nantes-Rennes Lidar Platform has been funded by the Region Pays de la Loire with funding of the RS2E-OSUNA programs and the Region Bretagne with support from the European Regional Development Fund. Patrick Launeau is greatly acknowledged for his contribution in the acquisition of the Titan DW sensor. We thank Cyril Michon, Emmanuel Gouraud, William Gentile from Geofit-Expert company, Paul Larocque and Anca Dorbinescu from Teledyne Optech and Laurence Hubert-Moy for their contribution in the overall operation of the Titan DW sensor. We thank Electricité De France (A. Barillier, A. Clutier) for commissioning the acquisition of the Ain river survey and providing access to the data. Daniel Girardeau-Montaut is greatly acknowledged for his ongoing development of Cloudcompare which has been used both for processing and figure generation in this work.

References

Abdallah, H., Baghdadi, N., Bailly, J., Pastol, Y., & Fabre, F. (2012). Wa-LiD : A New LiDAR Simulator for Waters. *IEEE Geosci. Remote Sensing Lett.*, *9*(4), 744–748. https://doi.org/10.1109/LGRS.2011.2180506

Allouis, T., Bailly, J.-S., Pastol, Y., & Le Roux, C. (2010). Comparison of LiDAR waveform processing methods for very shallow water bathymetry using Raman, near-infrared and green signals. *Earth Surface Processes and Landforms*, *650*(January). https://doi.org/10.1002/esp.1959

Bailly, J. S., le Coarer, Y., Languille, P., Stigermark, C. J., & Allouis, T. (2010). Geostatistical estimations of bathymetric LiDAR errors on rivers. *Earth Surface Processes and Landforms*, *35*(10), 1199–1210. https://doi.org/10.1002/esp.1991

Cossio, T., Slatton, K. C., Carter, W., Shrestha, K., & Harding, D. (2009). Predicting topographic and bathymetric measurement performance for low-SNR airborne lidar. *IEEE Transactions on Geoscience and Remote Sensing*, *47*(7), 2298–2315. https://doi.org/10.1109/TGRS.2008.2011054

Crowder, D. W., & Diplas, P. (2000). Using two-dimensional hydrodynamic models at scales of ecological importance. *Journal of Hydrology*, *230*(3–4), 172–191. https://doi.org/10.1016/S0022-1694(00)00177-3

Daniele, T., McKean, J., Benjankar, R. M., Wright, W., Goode, J. R., Chen, Q., et al. (2018). Mapping river bathymetries: evaluating topobathymetric LiDAR survey. *Earth Surface Processes and Landforms*. https://doi.org/10.1002/esp.4513

Davies-Colley, R. J., & Nagels, J. W. (2008). Predicting light penetration into river waters. *Journal of Geophysical Research: Biogeosciences*, *113*(3), 1–9. https://doi.org/10.1029/2008JG000722

Davy, P., Croissant, T., & Lague, D. (2017). A precipiton method to calculate river hydrodynamics, with applications to flood prediction landscape evolution models, and braiding instabilities. *J. Geophys. Res.*, *122*, 1–22. https://doi.org/10.1002/2016JF004156

Devlin, M. J., Barry, J., Mills, D. K., Gowen, R. J., Foden, J., Sivyer, D., & Tett, P. (2008). Relationships between suspended particulate material, light attenuation and Secchi depth in UK marine waters. *Estuarine, Coastal and Shelf Science*, *79*(3), 429–439. https://doi.org/10.1016/j.ecss.2008.04.024

Dietrich, J. T. (2017). Bathymetric Structure-from-Motion : extracting shallow stream bathymetry from multi-view stereo photogrammetry. *Earth Surf. Proc. Landforms*, *42*, 355–364. https://doi.org/10.1002/esp.4060

EDF R&D, T. P. (2011). CloudCompare (version 2.9) [GPL software]. Retrieved from http://www.danielgm.net/cc/.

Fernandez-Diaz, J. C., Glennie, C. L., Carter, W. E., Shrestha, R. L., Sartori, M. P., Singhania, A., et al. (2014). Early results of simultaneous terrain and shallow water bathymetry mapping using a single-wavelength airborne LiDAR sensor. *IEEE Journal of Selected Topics in Applied Earth Observations and Remote Sensing*, *7*(2), 623–635. https://doi.org/10.1109/JSTARS.2013.2265255

Fernandez-Diaz, J. C., Carter, W. E., Glennie, C., Shrestha, R. L., Pan, Z., Ekhtari, N., et al. (2016). Capability assessment and performance metrics for the titan multispectral mapping lidar. *Remote Sensing*, *8*(11), 1–33. https://doi.org/10.3390/rs8110936

Glennie, C. L., Carter, W. E., Shrestha, R. L., & Dietrich, W. E. (2013). Geodetic imaging with airborne LiDAR: the Earth's surface revealed. *Reports on Progress in Physics. Physical Society (Great Britain)*, *76*(8), 086801. https://doi.org/10.1088/0034-4885/76/8/086801

Guenther, G. C. (1985). Airborne laser hydrography: System design and performance factors. *NOAA Professional Paper Series*, *1*, 385.

Guenther, G. C., Cunningham, A. G., Larocque, P. E., & Reid, D. J. (2000). *Meeting the accuracy challenge in airborne lidar bathymetry*.

Hilldale, R. C., Raff, D., & Engineer, H. (2007). Assessing the ability of airborne LiDAR to map river bathymetry. *Earth Surface Processes and Landforms*, *33*(5), 773–783. https://doi.org/https://doi.org/10.1002/esp.1575

Höfle, B., Vetter, M., Pfeifer, N., Mandlburger, G., & Stötter, J. (2009). Water surface mapping from airborne laser. *Earth Surface Processes and Landforms*. https://doi.org/10.1002/esp

Joerg, P. C., Morsdorf, F., & Zemp, M. (2012). Uncertainty assessment of multi-temporal airborne laser scanning data: A case study on an Alpine glacier. *Remote Sensing of Environment*, *127*, 118–129. https://doi.org/10.1016/j.rse.2012.08.012

Lague, D., Brodu, N., & Leroux, J. J. (2013). Accurate 3D comparison of complex topography with terrestrial laser scanner: Application to the Rangitikei canyon (N-Z). *ISPRS Journal of Photogrammetry and Remote Sensing*, *82*, 10–26. https://doi.org/10.1016/j.isprsjprs.2013.04.009

Lassettre, N. S., Piégay, H., Dufour, S., & Rollet, A.-J. (2008). Decadal changes in distribution and frequency of wood in a free meandering river, the Ain River, France. *Earth Surface Processes and Landforms*, *33*, 1098–1112. https://doi.org/10.1002/esp.1605

Lee, Z., Shang, S., Lin, G., Liu, T., Liu, Y., Du, K., & Luis, K. (2017). Secchi disk observation with spectral-selective glasses in blue and green waters. *Optics Express*, *25*(17), 19878. https://doi.org/10.1364/OE.25.019878

Lee, Z., Shang, S., Du, K., & Wei, J. (2018). Resolving the long-standing puzzles about the observed Secchi depth Resolving the long-standing puzzles about the observed Secchi depth relationships. *Limnol. Oceanogr.* https://doi.org/10.1002/lno.10940

Legleiter, C. J., & Fonstad, M. A. (2012). An introduction to the Physical Basis for Deriving River Information by Optical Remote Sensing. In *Fluvial remote sensing for science and management* (pp. 43–69). Wiley-Blackwell.

Legleiter, C. J., Roberts, D. A., & Lawrence, R. L. (2009). Spectrally based remote sensing of river bathymetry. *Earth Surface Processes and Landforms*, *34*, 1039–1059. https://doi.org/10.1002/esp.1787

Legleiter, C. J., Overstreet, B. T., Glennie, C. L., Pan, Z., Fernandez-Diaz, J. C., & Singhania, A. (2016). Evaluating the capabilities of the CASI hyperspectral imaging system and Aquarius bathymetric LiDAR for measuring channel morphology in two distinct river environments. *Earth Surface Processes and Landforms*, *41*(3), 344–363. https://doi.org/10.1002/esp.3794

Lejot, J., Delacourt, C., Piégay, H., Fournier, T., Tremelo, M., & others. (2007). Very high spatial resolution imagery for channel bathymetry and topography from an unmanned mapping controlled platform. *Earth Surface Processes and Landforms*, *32*(11), 1705–1725. https://doi.org/10.1002/esp.1595

Leyland, J., Hackney, C. R., Darby, S. E., Parsons, D. R., Best, J. L., Nicholas, A. P., et al. (2017). Extreme flood-driven fluvial bank erosion and sediment loads: direct process measurements using integrated Mobile Laser Scanning (MLS) and hydro-acoustic techniques. *Earth Surface Processes and Landforms*, *42*(2), 334–346. https://doi.org/10.1002/esp.4078

Mallet, C., & Bretar, F. (2009). Full-waveform topographic lidar: State-of-the-art. *ISPRS Journal of Photogrammetry and Remote Sensing*, *64*(1), 1–16. https://doi.org/10.1016/j.isprsjprs.2008.09.007

Mandlburger, G., Pfennigbauer, M., & Pfeifer, N. (2013). Analyzing near water surface penetration in laser bathymetry - A case study at the River Pielach. *ISPRS Annals of Photogrammetry, Remote Sensing and Spatial Information Sciences*, *II-5/W2*(November), 175–180. https://doi.org/10.5194/isprsannals-II-5-W2-175-2013

Mandlburger, G., Hauer, C., Wieser, M., & Pfeifer, N. (2015). Topo-bathymetric LiDAR for monitoring river morphodynamics and instream habitats-A case study at the Pielach River. *Remote Sensing*, *7*(5), 6160–6195. https://doi.org/10.3390/rs70506160

McKean, J., Isaak, D. J., & Wright, C. W. (2008). Geomorphic controls on salmon nesting patterns

described by a new, narrow-beam terrestrial–aquatic lidar. *Frontiers in Ecology and the Environment*, *6*(3), 125–130. https://doi.org/10.1890/070109

McKean, J., Nagel, D., Tonina, D., Bailey, P., Wright, C. W., Bohn, C., & Nayegandhi, A. (2009). Remote sensing of channels and riparian zones with a narrow-beam aquatic-terrestrial LIDAR. *Remote Sensing*, *1*(4), 1065–1096. https://doi.org/10.3390/rs1041065

McKean, J., Tonina, D., Bohn, C., & Wright, C. W. (2014). Effects of bathymetric lidar errors on flow properties predicted with a multi-dimensional hydraulic model. *Journal of Geophysical Research: Earth Surface*, *119*(3), 644–664. https://doi.org/10.1002/2013JF002897

Nittrouer, J., Allison, M., & Campanella, R. (2008). Bedform transport rates for the lowermost Mississippi River. *Journal of Geophysical Research*, *113*(F3), 1–16. https://doi.org/10.1029/2007JF000795

Pan, Z., Glennie, C., Hartzell, P., Fernandez-Diaz, J., Legleiter, C. J., & Overstreet, B. (2015). Performance Assessment of High Resolution Airborne Full Waveform LiDAR for Shallow River Bathymetry. *Remote Sensing*, *7*(5), 5133–5159. https://doi.org/10.3390/rs70505133

Pan, Z., Glennie, C., Fernandez-Diaz, J. C., Shrestha, R., Carter, B., Hauser, D., et al. (2016). Fusion of bathymetric LiDAR and hyperspectral imagery for shallow water bathymetry. *International Geoscience and Remote Sensing Symposium (IGARSS)*, *2016-Novem*, 3792–3795. https://doi.org/10.1109/IGARSS.2016.7729983

Parsons, D. R., Best, J. L., Orfeo, O., Hardy, R. J., Kostaschuk, R., & Lane, S. N. (2005). Morphology and flow fields of three-dimensional dunes, Rio Paraná, Argentina: Results from simultaneous multibeam echo sounding and acoustic Doppler current profiling. *Journal of Geophysical Research: Earth Surface*. https://doi.org/10.1029/2004JF000231

Passalacqua, P., Belmont, P., Staley, D. M., Simley, J. D., Arrowsmith, J. R., Bode, C. a., et al. (2015). Analyzing high resolution topography for advancing the understanding of mass and energy transfer through landscapes: A review. *Earth-Science Reviews*, *148*, 174–193. https://doi.org/10.1016/j.earscirev.2015.05.012

Richter, K., Maas, H. G., Westfeld, P., & Weiß, R. (2017). An Approach to Determining Turbidity and Correcting for Signal Attenuation in Airborne Lidar Bathymetry. *Photogrammetrie, Fernerkundung, Geoinformation*, *85*(1), 31–40. https://doi.org/10.1007/s41064-016-0001-0

Saylam, K., Brown, R. A., & Hupp, J. R. (2017). Assessment of depth and turbidity with airborne Lidar bathymetry and multiband satellite imagery in shallow water bodies of the Alaskan North Slope. *International Journal of Applied Earth Observation and Geoinformation*, *58*, 191–200. https://doi.org/10.1016/j.jag.2017.02.012

Tarolli, P. (2014). High-resolution topography for understanding Earth surface processes: Opportunities and challenges. *Geomorphology*, *216*, 295–312. https://doi.org/10.1016/j.geomorph.2014.03.008

Vosselman, F., & Maas, H. G. (2010). *Airborne and terrestrial laser scanning*. CRC.

Wagner, W., Lague, D., Mohrig, D., Passalacqua, P., Shaw, J., & Moffett, K. (2017). Elevation change and stability on a prograding delta. *Geophysical Research Letters*, *44*(4), 1786–1794. https://doi.org/10.1002/2016GL072070

Westaway, R. M., Lane, S. N., & Hicks, D. M. (2000). The development of an automated correction procedure for digital photogrammetry for the study of wide, shallow, gravel-bed rivers. *Earth Surface Processes and Landforms*, *25*(2), 209–226.

Williams, R. D., Brasington, J., Vericat, D., & Hicks, D. M. (2014). Hyperscale terrain modelling of braided rivers: Fusing mobile terrestrial laser scanning and optical bathymetric mapping. *Earth Surface Processes and Landforms*, *39*(2), 167–183. https://doi.org/10.1002/esp.3437

Woodget, A. S., Carbonneau, P. E., Visser, F., & Maddock, I. P. (2015). Quantifying submerged fluvial topography using hyperspatial resolution UAS imagery and structure from motion photogrammetry. *Earth Surface Processes and Landforms*, *40*(1), 47–64. https://doi.org/10.1002/esp.3613

Wu, J., Van Aardt, J. A. N., McGlinchy, J., & Asner, G. P. (2012). A robust signal preprocessing chain for small-footprint waveform LiDAR. *IEEE Transactions on Geoscience and Remote Sensing*, *50*(8), 3242–3255. https://doi.org/10.1109/TGRS.2011.2178420

Zhao, X., Zhao, J., Zhang, H., & Fengnian, Z. (2018). Remote Sensing of Sub-Surface Suspended Sediment Concentration by Using the Range Bias of Green Surface Point of Airborne LiDAR Bathymetry. *Remote Sensing*, *10*(681). https://doi.org/10.3390/rs10050681